

# Supplemental material to “Timescales in creep and yielding of attractive gels”

Vincent Grenard, Thibaut Divoux, Nicolas Taberlet, and Sébastien Manneville

## 1 Procedure for removing spurious scattering from the cell walls

In the present work, the Plexiglas cylinders used in our Couette geometry were sand-blasted in order to provide a roughness of about  $1 \mu\text{m}$  which leads to significant scattering of the incident ultrasonic pulses. This results in spurious fixed echoes in the raw ultrasonic data that get mixed with the echoes backscattered by the moving particles. Such fixed echoes appear as vertical lines in the spatiotemporal diagram of Supplemental Figure 1(a) that shows the successive pressure signals  $p(t_{us}, t)$  coded in gray levels as a function of the ultrasonic time-of-flight  $t_{us}$  (horizontal axis) after a single pulse is sent at time  $t$  (vertical axis). Using the cross-correlation algorithm described in Ref.<sup>1</sup> on such raw ultrasonic data leads to a dramatic underestimation of the local velocities at the location of these fixed echoes.

In order to remove the undesired fixed echoes before data analysis, we average the ultrasonic signals recorded during the systematic preshear step at  $\dot{\gamma}_p = 10^3 \text{ s}^{-1}$  (see Sect. 2.3) and subtract this average to each raw pressure signal recorded subsequently during the actual experiment. The result is shown in Supplemental Figure 1(b). In the averaging process at large shear rate, all contributions from acoustic scatterers within the sheared fluid cancel out and one is left with the static spurious signal. Subtracting this signal to the raw data appears as a very efficient way to remove the spurious contributions of the ultrasonic waves scattered off by the surface roughness of the outer fixed wall.

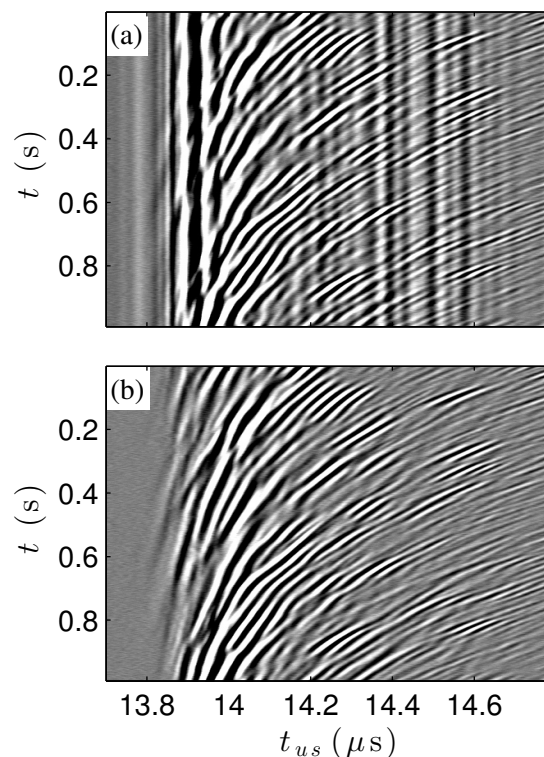


**Fig. 1** Spatiotemporal diagrams of the pressure signal recorded as a function of time  $t_{us}$  (horizontal axis) after a single pulse is sent at time  $t$  (vertical axis). (a) Raw data. (b) Same data after fixed echoes have been removed following the procedure described in the text. The pressure signal is coded in linear gray levels.

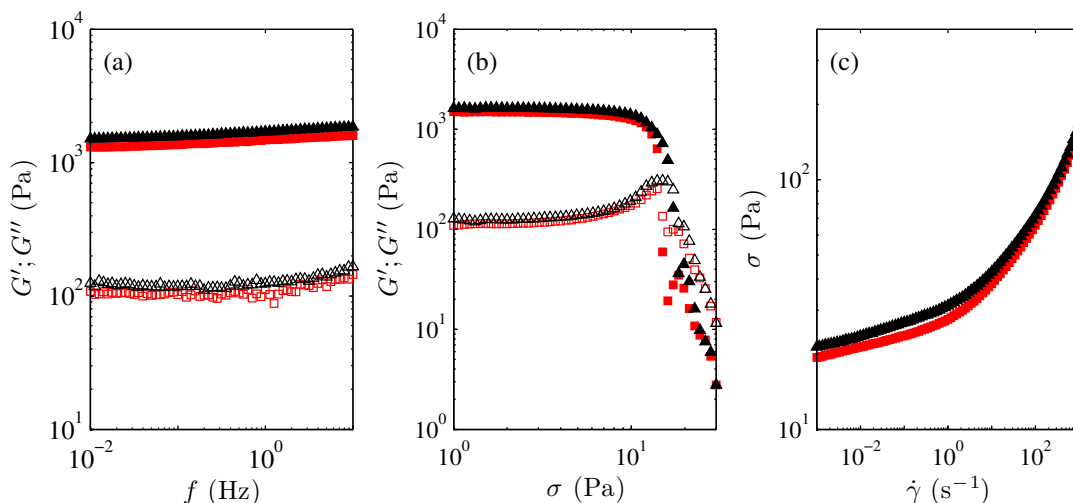


**Fig. 2** Rheological properties of a CB gel at 6% w/w seeded with 1% w/w hollow glass microspheres (black triangles) compared to those of the same sample free of seeding microspheres (red squares). Viscoelastic moduli  $G'$  (filled symbols) and  $G''$  (empty symbols) (a) as a function of frequency  $f$  for a stress amplitude of 2 Pa (waiting time of 6 oscillation periods per point) and (b) as a function of stress amplitude  $\sigma$  at a frequency of 1 Hz (waiting time of 5 s per point). (c) Flow curves  $\sigma$  vs  $\dot{\gamma}$  measured by decreasing  $\dot{\gamma}$  (waiting time of 1 s per point).

## 2 Influence of adding acoustic contrast agents to carbon black gels

Supplemental Figure 2 compares the linear and nonlinear rheological properties of 6% w/w CB gels with and without acoustic contrast agents, namely 1% w/w hollow glass microspheres of mean diameter  $6 \mu\text{m}$  (Spherical, Potters) and density  $1.1 \text{ g.cm}^3$ . Addition of acoustic contrast agents does not significantly affect the mechanical behaviour of CB gels. Quantitatively, we note that the viscoelastic moduli at rest increase by about 10% upon addition of microspheres [see Supp. Fig. 2(a,b)]. Such an enhancement of the viscoelastic properties is expected and has already been observed in, e.g., carboxypol microgels<sup>2</sup>. Accordingly, the flow curve of a CB gel as well as the yield stress are shifted upwards by about 10% when adding 1% w/w hollow glass microspheres to the system [see Supp. Fig. 2(c)].

## 3 Influence of the preshear protocol on the fluidization time

The fluidization time  $\tau_f$  was measured as described in the main text after preshearing a 6% w/w CB gel either at  $+1000 \text{ s}^{-1}$  or at  $-1000 \text{ s}^{-1}$  for 20 s before viscoelastic moduli at rest are monitored for 300 s and a given stress  $\sigma$  is subsequently applied in the positive direction. As shown in Supplemental Figure 3 this leads to significant differences in the yielding phenomenon. In both cases, an exponential behaviour is found for  $\tau_f$  vs  $\sigma$  but fluidization is much faster when creep

and preshear are applied in opposite directions.

We checked that:

- (i) the preshearing direction does not affect the shape of the subsequent shear rate response  $\dot{\gamma}(t)$  (data not shown), which remains similar to the responses shown in Fig. 4 in the main text and, in particular, shows three well-defined regimes.
- (ii) reversing both preshear and creep directions does not affect  $\tau_f$  so that the difference may not be attributed to an artifact

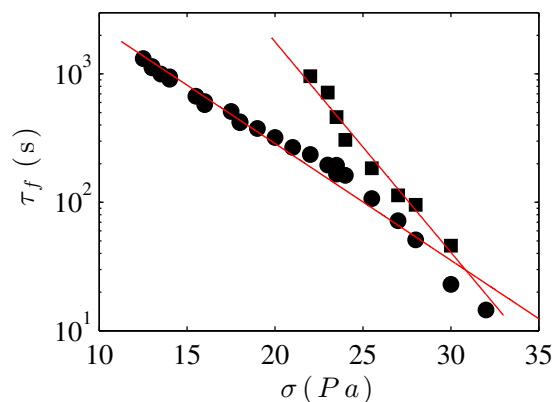


**Fig. 3** Fluidization time  $\tau_f$  after two different preshear protocols for a 6% w/w CB gel under rough boundary conditions: preshear for 20 s at  $+1000 \text{ s}^{-1}$  (■) and at  $-1000 \text{ s}^{-1}$  (●). The shear stress  $\sigma$  is applied in the positive direction once viscoelastic moduli have been measured for 300 s after preshear. Red lines are the best exponential fits  $\tau_f = \tau_0 \exp(-\sigma/\sigma_0)$ .

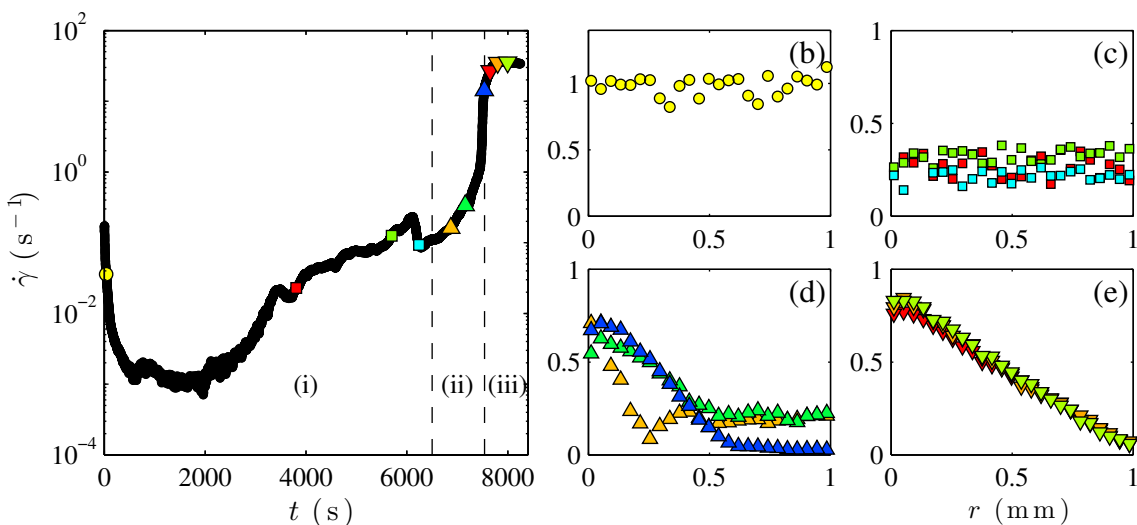


**Fig. 4** Creep experiment in a 6% w/w CB gel at  $\sigma = 16$  Pa under smooth boundary conditions. (a) Shear rate response  $\dot{\gamma}(t)$ . The vertical dashed lines indicate the limits of the three regimes discussed in the text. The coloured symbols show the times at which the velocity profiles in (b)–(e) are recorded. Velocity profiles  $v(r, t_0)$ , where  $r$  is the distance to the rotor, normalized by the current rotor velocity  $v_0(t_0)$  at (b)  $t_0 = 39$  s, (c)  $t_0 = 3806, 5700$ , and  $6240$  s, (d)  $t_0 = 6871, 7157$ , and  $7536$  s, and (e)  $t_0 = 7650, 7800$ , and  $8000$  s.

due to our rheometer or geometry,

(iii) in the case of successive preshears with different directions such as in the protocol used in the main text ( $+1000 \text{ s}^{-1}$  followed by  $-1000 \text{ s}^{-1}$ ), the fluidization time is only affected by the last preshear step.

This clearly shows that, even though preshear successfully erases previous sample history, the resulting gel microstructure is sensitive to preshear.

The influence of preshear was investigated by Osuji *et al.*<sup>3</sup> in CB gels in tetradecane at 2–8% w/w. A power-law dependence of the elastic modulus with the shear stress applied during preshear was reported together with a slow decrease of the residual “internal stress”, i.e. the shear stress measured after flow cessation,  $\sigma_i(t) \sim t^{-0.1}$ . These findings were interpreted based on a simple model for the cluster size reached after preshearing at a stress  $\sigma_p$  and on an unusually fast build-up of the network structure after cessation of shear in which internal stresses act opposite to the preshear direction.

Internal stresses may partly explain our results. Indeed, if stress is applied in the direction opposite to preshear, internal stress adds up to the applied stress, thus facilitating yielding and leading to a faster fluidization process. Yet Supplemental Figure 3 shows that the effect of preshear is not simply an effective change of  $\sigma$  by a constant  $\pm\sigma_i$  depending on the preshear direction since in this case the two curves  $\tau_f$  vs  $\sigma$  would only be translated by a constant amount. Moreover, if the differences in fluidization times were to be explained solely by internal stresses, then one would expect that for very long fluidization times (i.e. for small  $\sigma$ ), the slow relaxation

of internal stresses leads to smaller discrepancies in  $\tau_f$ . This is not observed in our data. Rather, fluidization times become similar for large values of  $\sigma$  and both parameters  $\sigma_0$  and  $\tau_0$  in the exponential fits depend on the preshear direction. We find  $\sigma_0 = 2.6$  Pa and  $\tau_0 = 3.4 \cdot 10^6$  s for a preshear in the positive direction and  $\sigma_0 = 4.8$  Pa and  $\tau_0 = 1.9 \cdot 10^4$  s for the opposite direction (see red lines in Supp. Figure 3). This suggests that the anisotropy of the gel structure induced by preshearing plays an important role in the delayed fluidization under creep. Such an anisotropy is not accounted for in the model of Ref.<sup>4</sup>.

#### 4 Velocity profiles under smooth boundary conditions

Supplemental Figure 4 reports velocity profiles recorded during a creep experiment performed under smooth boundary conditions on a 6% w/w CB gel together with the corresponding evolution of the shear rate  $\dot{\gamma}(t)$  [see Supp. Figure 4(a)]. Total slippage at the fixed outer wall is observed as soon as shear is applied at  $t = 0$  [see Supp. Fig. 4(b)]. Although velocities for  $200 \lesssim t \lesssim 3000$  s are too small to allow for reliable measurements, the flow is most likely pluglike throughout the creeping flow regime (i) with slip velocities increasing at the rotor and decreasing at the stator. Indeed, once the shear rate has raised above roughly  $10^{-2} \text{ s}^{-1}$  allowing velocities to be accurately estimated, velocities show a flat profile with almost total slippage at the rotating inner wall [see Supp. Fig. 4(c)]. After a small bump in  $\dot{\gamma}(t)$  which is characteristic of the shear

rate response in a smooth cell (here at  $t \simeq 6000$  s, see also Fig. 10 in the main text), highly fluctuating shear-banded velocity profiles are recorded [regime (ii), see Supp. Fig. 4(d)]. Steady homogeneous velocity profiles are recovered after the inflection point in  $\dot{\gamma}(t)$ , with about 10% of residual wall slip at the rotor [regime (iii), see Supp. Fig. 4(e)].

## 5 Evolution of the characteristic shear rate $\dot{\gamma}^*$ after failure at the inner wall

The characteristic shear rate  $\dot{\gamma}^*$  after failure at the inner wall at  $t = \tau_c$  under rough boundary conditions is shown in Supplemental Figure 5 as a function of the applied shear stress  $\sigma$  for four gel concentrations  $C$ .  $\dot{\gamma}^*$  is seen to increase fairly linearly with the applied stress  $\sigma$  and, on average, to increase with the gel concentration  $C$ .

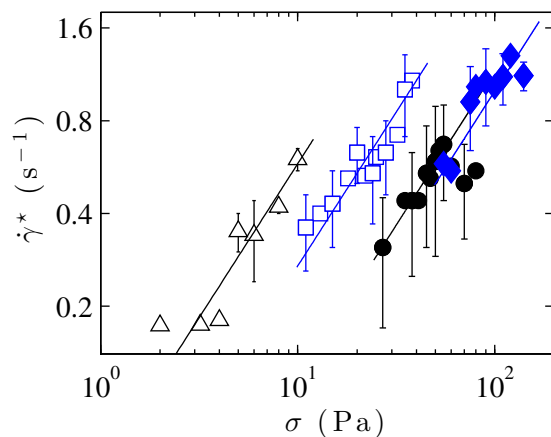


**Fig. 5** Shear rate  $\dot{\gamma}^*$  after failure at the inner wall at  $t = \tau_c$  as a function of the applied shear stress  $\sigma$  for CB gels of concentration  $C = 4$  ( $\triangle$ ),  $6$  ( $\square$ ),  $8$  ( $\bullet$ ), and  $10\%$  w/w ( $\blacklozenge$ ). Solid lines correspond to linear behaviours  $\dot{\gamma}^* \propto \sigma$ . Error bars show the variations of  $\dot{\gamma}(t)$  over the shear rate plateau for  $\tau_c < t < \tau_f$ .

## 6 Shear rate response as a function of strain

Supplemental Fig. 6 shows the data of Fig. 6 replotted as a function of the strain  $\gamma$ . The good collapse of all curves at the end of the initial creep regime (see also inset of Supp. Fig. 6) suggests that failure at the inner wall at  $\tau_c$  can be associated with a characteristic “yield strain”  $\gamma_c \simeq 0.2$ – $0.3$ . The strains  $\gamma_f$  corresponding to full fluidization at  $\tau_f$  are spread over a very large range  $\gamma_f \simeq 200$ – $3000$ .

## References

- 1 S. Manneville, L. Bécu and A. Colin, *Eur. Phys. J. AP*, 2004, **28**, 361–373.
- 2 T. Divoux, C. Barentin and S. Manneville, *Soft Matter*, 2011, **7**, 9335–9349.
- 3 C. O. Osuji, C. Kim and D. A. Weitz, *Phys. Rev. E*, 2008, **77**, 060402(R).
- 4 S. B. Lindström, T. E. Kodger, J. Sprakel and D. A. Weitz, *Soft Matter*, 2012, **8**, 3657–3664.

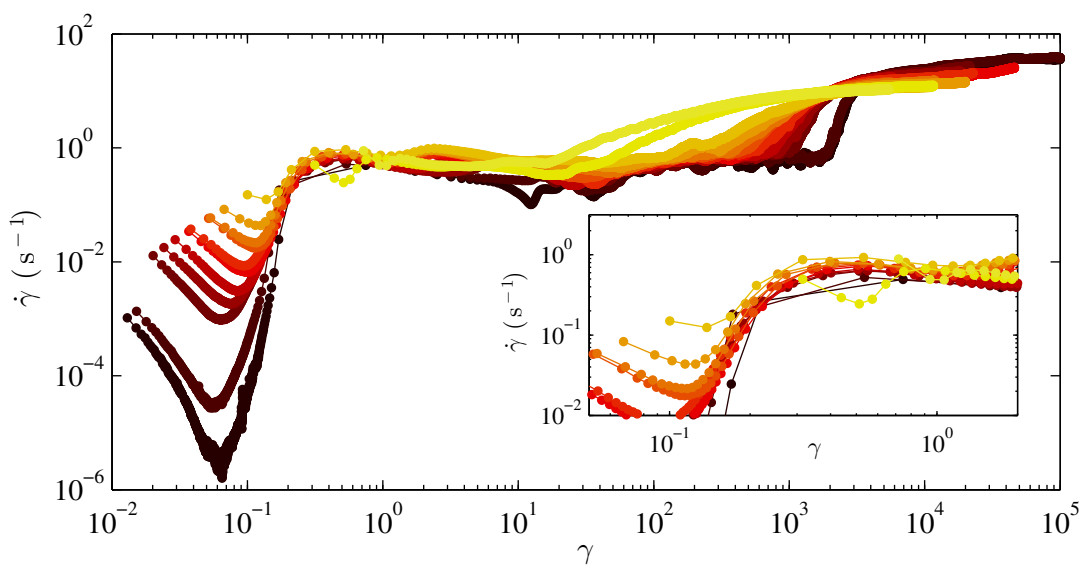


**Fig. 6** Creep experiments in an 8% w/w CB gel under rough boundary conditions. Shear rate responses  $\dot{\gamma}$  as a function of the strain  $\gamma$  for different shear stresses  $\sigma$  applied at time  $t = 0$ : from right to left,  $\sigma = 24, 27, 35, 38, 41, 45, 47, 50, 52, 55, 60, 70,$  and  $80$  Pa. Inset: enlargement over the end of the initial creep regime.